

# Post-processing of customized implants made by laser beam melting from pure Titanium

C. COSMA<sup>a\*</sup>, N. BALC<sup>ad</sup>, M. MOLDOVAN<sup>b</sup>, L. MOROVIC<sup>c</sup>, P. GOGOLA<sup>c</sup>, C. MIRON-BORZAN<sup>ad</sup>

<sup>a</sup>Technical University of Cluj-Napoca, Faculty of Machine Building, Cluj-Napoca, Romania

<sup>b</sup>Babes-Bolyai University, Raluca Ripan Institute for Research in Chemistry, Cluj-Napoca, Romania

<sup>c</sup>Slovak University of Technology in Bratislava, Faculty of Materials Science and Technology in Trnava, Slovakia

A major problem in laser beam melting is to post-process the complex surfaces. The objective of this research was to investigate the influence of three combined post-processing methods on customized implants manufactured by selective laser melting, focusing on complex contact surfaces between the parts and support structures. These anatomical contact shapes are the most difficult areas to be post-processed. The results showed that the roughness is reduced, the obtained surfaces are homogenous, and deviations between  $\pm 0.12\text{mm}$  could be expected. This study provides cases references for designing, directly manufacturing by Nd:YAG solid laser and post-processing of medical implants made from titanium powder.

(Received September 27, 2017; accepted November 28, 2017)

**Keywords:** Selective laser melting, Pure titanium, Implant, Accuracy, SEM investigation

## 1. Introduction

The technological evolution has contributed to the continuous modernization with a fast rhythm of the laser beam melting (LBM) process. This rapid manufacturing of metal parts has been applied successfully in medicine [1], [2], [3], [4], [5], [6] and industry [7]. The continuous growth and the increased application of LBM have also attracted new research interest and developments in metal powder production [8]. LBM process facilitate the directly production of customized implants from various laser materials [2]. Due to the high performance of the implants LBM processed, sometimes they are exceeding their conventionally manufactured counterparts [9], [10].

In the last years, using the selective laser melting process (SLM), customized implants have been made and have been applied in medical complex bone reconstructions, that until then, seemed to be unsolvable medical cases, being considered international premieres. This involves the complete replacement of the mandible with an implant [9] and the substitution of the deficient zygomatic bone with a mirror reconstruction of the healthy bone [11].

In order to minimize the risk of implant rejection, various research teams have manufactured implants with physical-mechanical characteristics similar to the host bone [12]. Furthermore, through the development of the geometrically defined interconnected pores ("lattice structures") inside the parts, a prosthesis was made to treat a total knee arthroplasty [9]. These lattice structures allow the development (at the interface between the implant and the bone) of new tissues that strongly anchor the metal structure inside the surgical site [2], [13]. The results of these surgeries are acceptable, the implants being perfectly

integrated without any sign of rejection, contributing to the improvement of the patients' health and to their reintegration into the community.

To obtain these remarkable results, the anchor of the parts with supports during SLM processing was needed. These structures not only prevent the deformation of implants caused by the material's shrinkage, but also maintain the manufacturing stability during the SLM process [14]. It is also known that, the contact surface between the parts and the supports which anchor it, suffers a lot in quality terms (roughness and accuracy) [15]. However, there are few study regarding this issue, most of them are focused on analyzing the influence of processing parameters on outer surfaces quality which were not anchored with supports structures [16], [17], [18], [19]. Usually, these surfaces are deteriorated in terms of quality and are difficult to be cleaned. An efficient post-processing method especially addressed to these surfaces is required. Even more, a good understanding of post-processing impact on these surfaces is needed, because the contact surfaces between the parts and supports represents a major problem of parts processed by LBM technology.

Besides monitoring and controlling the LBM process itself, understanding of the relationship between the post-processing and the obtained surface quality is required. The aim of this study was to analyze the influence of three post-processing methods on the surface quality of medical implants manufactured through SLM, focussing on complex contact shapes between the parts and support structures. The post-processing methods targeted were: alumina sandblasting, carborundum polishing and ultrasonication in isopropyl alcohol. The influence of these cleaning techniques on surfaces was investigated morphologically and compositionally via Scanning

Electron Microscopy (SEM) and Energy-Dispersive X-ray Spectroscopy (EDX). By optical scanning of the manufactured implants, three dimensional surface deviation maps were created in order to inspect the accuracy of complex shapes. The obtained results provide two case references for directly manufacturing and post-processing of customized implants (without any stress relieved treatment), that could be applied in maxillofacial surgery and total knee arthroplasty.

## 2. Materials and Methods

### 2.1. Material selection

Titanium is intensively used in surgery due to a good biocompatibility, being explained by its physical-mechanical properties and by the fact that the metal surface is always coated with a  $TiO_2$  layer [20]. This nanometric layer is responsible for the corrosion resistance [21] and bioinert behaviour *in vivo*, leading to an acceptable osseointegration [11]. In the literature, there are few published researches regarding the processing by SLM of implants from pure Ti Grade I powder [22], most of them are referring to Ti Grade II-IV powder (up to 99.2% Ti) [11] or  $Ti_6Al_4V$  alloy [23]. For this reason, the laser material used for the SLM processing of implants was Ti.

Today, metal powder for LBM is mainly developed by gas atomization method. During this process, the liquid metal is atomized (due to inert gas jets) into fine metal droplets which cool down during their fall in the atomizing tower. Metal powders obtained by gas-atomization offer a perfectly spherical shape and a high cleanliness level. The Ti powder used in this research was developed by gas-atomized and provided by Osaka Titanium Technologies (Japan). This Ti powder is named TILOP 45, has  $45\mu m$  particles diameter, the melting point around  $1670^\circ C$ , and it can be included in the category of pure Ti Grade I (99.5% Ti).

### 2.2. Designing the zygomatic reconstruction and knee replacement implant

The first task of this study was to design two customized medical implants for two distinct areas, such as maxillofacial area (zygomatic bone reconstruction) and orthopedic area (more exactly for treating a total knee arthroplasty by applying a prosthesis that has lattice structures in the tibial component).

Any bone reconstruction, starts with processing the CT images of patient, created a link between medicine and engineering [24]. In this study, the CT images of a 57 years old, volunteer patient were processed in MIMICS software. The virtual model of zygomatic implant (Fig. 1) was designed in Creo Parametric software.

The knee prosthesis is used to relieve pain, correcting leg deformity, and facilitates the resumption of normal activities. Total knee arthroplasty is the surgical intervention by which the prosthesis system is inserted into

the body. The particularity of this tibial component design is lattice structures applied on femoral component.

To manufacture this scaffold structures LBM systems are required because they cannot be achieved by conventional technologies.

Moreover, interconnected pore structures facilitate fluid penetration and the penetration of bone cells, leading to a gradual growth of tissues at the same time with their fixation onto the respective structure [9], [25], [26], [27]. Fig. 2 presents the virtual model of tibial component, designed in Creo Parametric software. These macro-porous networks could support the vascular system necessary for a continuous bone development [28], [29]. These macro-porous structures could favour the vascularization or transport of the metabolic products, improving the osseointegration [30], [31]. The pore size designed and applied to this tibial component was  $1.10mm$ .

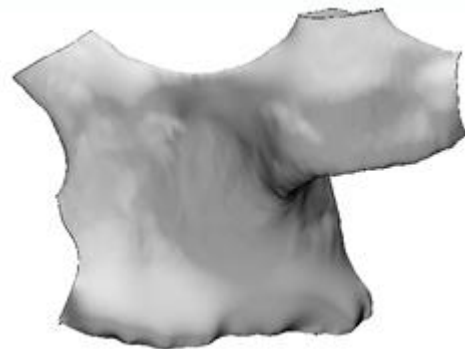


Fig. 1. The virtual zygomatic implant

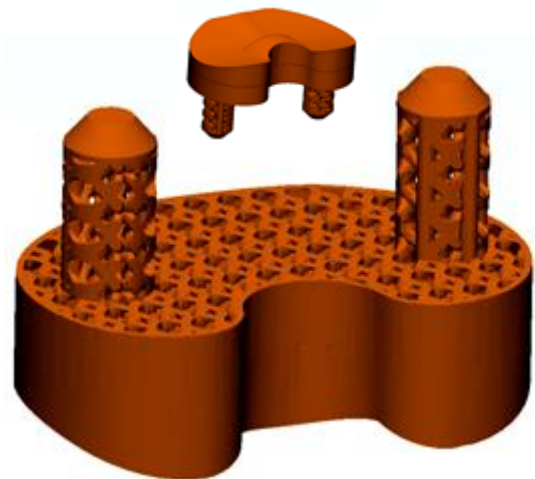


Fig. 2. The virtual tibial component with lattice structures

### 2.3. SLM processing of customized implants

To manufacture the implants from pure Ti powder, the SLM REALIZER 250 equipment (SLM Solutions GmbH, Germany) was used. The system uses selective laser melting technology and can manufacture three-

dimensional metal parts by fusing fine metallic powders together slice by slice, under a protective high-purity argon atmosphere. This technology uses a solid-state laser type Nd:YAG (neodymium-doped yttrium aluminum garnet  $\text{Nd}^{3+}:\text{Y}_3\text{Al}_5\text{O}_{12}$ ) and the maximum power of the laser beam is 200 W. The properties of Nd:YAG laser are as follows: 1064 nm emission wavelength in infrared spectrum, 230  $\mu\text{s}$  duration of fluorescence, none birefringence (only thermally induced),  $0.14 \cdot \text{W} \cdot \text{cm} \cdot \text{K}^{-1}$  thermal conductivity,  $6.9 \cdot 10^{-6} \cdot \text{K}^{-1}$  thermal expansion coefficient and  ${}^4\text{F}_{3/2} \rightarrow {}^4\text{I}_{11/2}$  transition of energy (see Fig. 3). Due to the higher quantum efficiency and the lower heat generation under thermally boosted pumping, an all-solid-state Nd:YAG laser operating at 1064nm with high efficiency, high beam quality and high resonator stability can be achieved by thermally boosted pumping under the condition of optimizing the input data [32].

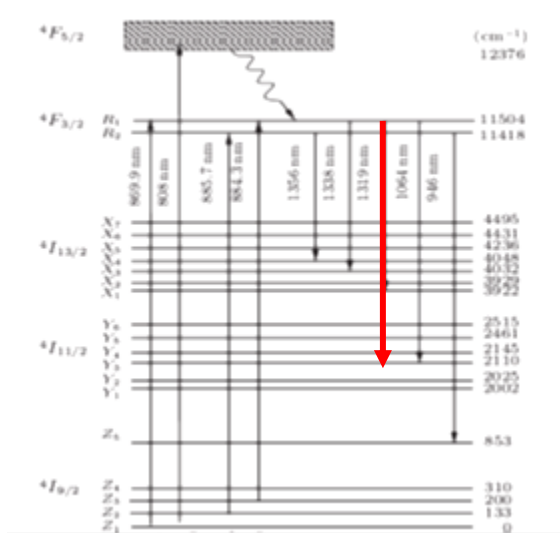


Fig. 3. Energy level diagram of Nd:YAG solid lasers [32]

In this research, when the laser irradiates the titanium powder, its scattering is eligible for the Mie theory [33]. Based on the Mie theory, when a parallel light with an intensity of  $I_0$  irradiates on isotropic spherical granules, the scattered light intensity at  $x$  distance from the diffuser is:

$$I = \frac{\lambda^2}{8\pi^2} \cdot \frac{i_1 + i_2}{x^2} I_0, \quad (1)$$

where  $\lambda$  is the wavelength of the incident light;  $i_1$  is the light intensity that the vibration is vertical to the plane of the incident light and the scattered light;  $i_2$  is the light intensity that the vibration is parallel to the plane of the incident light and the scattered light [33].

Even if Nd:YAG lasers are the most commonly used solid-lasers, in-depth studies are needed to process proper parts, especially on programming the process parameters for each metal powder.

In the previous developed studies, the optimal input data of SLM process were obtained [34]. The processing parameters used for pure Ti powder are: 120W laser

power, 500 mm/s scanning speed of laser and 50 $\mu\text{m}$  layer thickness of powder [34]. The energy input of each hatch scanning was calculated at  $43.63\text{J}/\text{mm}^3$  (according to density energy equation [35]). In order to reduce the surface roughness, previous studies have shown that the optimal SLM parameters for scanning the outer border of the parts are 133 W laser power and 344mm/s scanning speed of laser [36]. Also, to avoid the warpage effect, the implants were oriented at an angle of  $40^\circ$  between the main axis of the parts and the SLM base plate [15]. In order to easily remove the implants from the base plate, the supports were designed according to literature [14], [37]. With these settings of processing parameters, the designed customized implants were manufactured.

#### 2.4. Post-processing and surface characterization

After manually removing of support structures from the outer curved surface, the implants were post-processed using three methods, such as: alumina sandblasting, carborundum polishing and ultrasonication.

A common practice to clean metal surfaces is sandblasting with alumina (aluminum oxide) [38], hydroxyapatite [39], zirconia [40] or silicon dioxide [41]. The sandblasting is intended to polish the implants surfaces. In this study, the sandblasting of the samples was performed with alumina having a particle size of 120  $\mu\text{m}$ , at a pressure of 4 bars, the distance between the nozzle and the sample being 50 mm, at an angle of  $45^\circ$ . The main characteristics of the used alumina are 1450 HV hardness, 2072 $^\circ\text{C}$  melting point and 3.9  $\text{g}/\text{cm}^3$  density.

The polishing was done with carborundum abrasive discs mounted on an electric dental micro-motor at 1500rpm. Carborundum, also known as silicon carbide (SiC), is an abrasive with 1875 HV hardness, 3.21  $\text{g}/\text{cm}^3$  density and 2730 $^\circ\text{C}$  melting point.

Ultrasonication was performed in a RayPa UCI-50 (Espinar) bath, where the implants were sanked into isopropyl alcohol at 35 $^\circ\text{C}$ , for 30 minutes, at a frequency of 17 kHz. In the end, the samples were washed with distilled water and dried with hot air.

After the parts were post-processed, the roughness  $R_a$  was measured using a digital apparatus (Mitutoyo SJ-2010), according to ISO 4287:2001, where  $R_a$  is arithmetic average of absolute values.

The structural and morphological aspects of the post-processed complex shapes were investigated by scanning electron microscopes (SEM). The microscopes used were JEOL 7600F and Hitachi S-2600N and images of implants it were recorded by scanning the surface with a focused beam of electrons. The electrons interact with implant's atoms, generating signals that contain information about the surface topography and composition. The accelerating voltage set up was between 15-30kV and it is mentioned in the footnote of every picture. After post-processing, the implants were mounted in the sample holder and subsequently introduced into microscopes. Firstly, the implants were investigated after sandblasting technique and secondly in the end of all post-processing steps. The

surfaces were analyzed with an energy-dispersive spectroscope (EDX) incorporated in SEM.

## 2.5. Scanning and geometrical inspection

The geometrical inspection of the anatomical shape SLM-manufactured was carried out, based on the methodology didn't exceeded  $\pm 0.50$  mm. The geometrical inspection in this case means that the surface geometry of the designed model was compared with the SLM-manufactured implant. To develop a correct comparison diagram between the designed model and the manufactured implant, the 3D models of implants were converted in .STL files with a fine mesh. The digital zygomatic implant was obtained by dividing in 65,310 tetrahedral solid elements connected in 32,657 nodes. Also, the 3D model of the tibial component was converted into .STL file, and was divided in 90,984 tetrahedral connected in 41,994 nodes. These .STL files with the designed implants were set as reference models in comparison diagrams.

For 3D digitization of the processed implants, the non-contact optical 3D scanner GOM ATOS II TripleScan SO MV100 was used. The measuring principle of the 3D scanner is the active triangulation – fringe projection (structured light). The resolution of the 3D scanner's cameras are 5Mpix and the measuring volume MV100 (L x W x H: 100mm x 75mm x 70mm) was used. In the listed configuration, the measuring point distance is 0.04509 mm. To align the reference designed implant and the 3D scanned model, the method "best-fit" was used in the GOM ATOS Professional v7.5 SR2 software [42], [43].

## 3. Results and discussions

### 3.1. Implants processed by SLM

The normal lasing and terminal levels of LBM are  $^4F_{3/2}$  and  $^4I_{11/2}$ . The terminal laser level is  $2110\text{cm}^{-1}$  above the ground state (see Figure 3). At room temperature, almost all the ions transferred from the ground level to the pump bands end up in the upper laser level, having a fluorescent efficiency up to 99.5% and a radiative lifetime of  $230\ \mu\text{s}$  [44]. The process indicates that the pump laser of 1064nm boosted thermally and activated ions from the  $R_1$  sublevel of the  $^4F_{3/2}$  directly to the  $Y_3$  sublevel of the  $^4I_{11/2}$ . Maintaining a constant temperature at  $40^\circ\text{C}$ , the 1064 nm line in Nd:YAG is homogeneously broadened by thermally activates lattice vibrations. Also, the Nd:YAG crystal is the most widely-used laser gain medium because of its excellent optical and mechanical properties [45].

Without optimizing the process parameters of SLM process, heat generation would lead to thermal stress, stress birefringence and thermal lens effect that could limit the average output power and efficiency of laser emission and decrease the beam quality [32]. In order to limit these effects, all the SLM process parameters were optimized for Ti powder and they were mentioned above.

The virtual implants were processed at 1:2 scale (see Figure 4). With these SLM process parameters, the physical-mechanical characteristics of the pure Ti implants are: 101 GPa Young modulus, 0.3 Poisson's ratio, 210MPa yield strength and 410 MPa ultimate tensile strength [34], [46]. The processing time was diminished by orienting the pieces on the plate so that to reduce the height (see Figure 4b), and the thickness of a layer powder was  $50\ \mu\text{m}$ . The optimal modelling of the supports led to a slight removal of them from the contact surfaces. Figure 4a illustrates lattice supports that anchored the zygomatic implant and block supports that firmly secured the knee prosthesis on base plate. It should be noted that the optimal configuration of the SLM process parameters led to a good processability and the manufactured implants do not need stress relieved treatment. The SLM process was stable, lasted approx. 5h, and the implants did not visibly deform after removing them from the base plate. These implants have not undergone a thermal treatment to relieve the residual stress.

Depending on the area where they will be applied and on their functionality, the endosseous implants should take into account the bone structure that will be replaced because it has been shown that the rate of osseointegration is much higher in the area of the trabecular bone compared to the cortical bone [25]. For this reason, the processed knee prosthesis has a macro-porous interconnected structure in the trabecular bone area. Due to the anisotropic structure and the ability of the lattice structures to absorb shocks (Figure 4b), they can be successfully used not only in the medical implants but also in the automotive or aeronautic industry [47], [48], [49].

### 3.2. SEM and EDX investigations

The SEM and EDX analyses were mainly focussed on surfaces where the implants were anchored to the supports, knowing that these areas are very difficult to be post-processed [15]. Thus, these investigated areas were highlighted in Figure 4 by red squares.

The SEM images from Figure 5 are showing the initial surfaces produced by SLM at different magnification. It is known that the SLM-manufactured parts are susceptible to major defects and unfavourable issues like balling effect, microscopic and macroscopic cracks, heat affected zone, atmospheric conditions, residual stress phenomena or un-melted areas [49], [50], [51]. The obtained Ti surfaces have asymmetric streaks and scratches, or micro-pores (Figure 5). From this topographic analysis we find out that the melted track is continuous, uniform and does not show a light surface crack or deep cracks. A very important aspect is given by semi-melted Ti granules which are found on the surface (Fig. 5b). These spherical or elliptical granules have emerged from the balling effect phenomenon. Balling effect represents a fragmentation or droplets resulted from the melt pool due to the capillar instability and it is an undesirable phenomenon related to the laser-based processing [50].

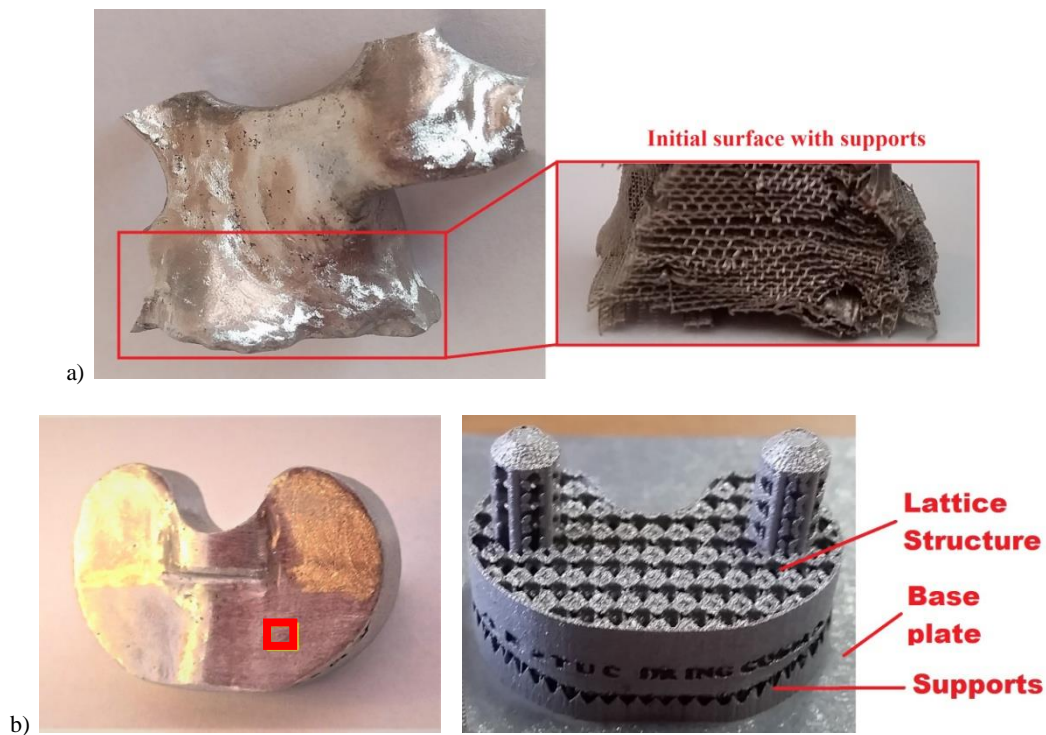


Fig. 4. Contact surface between implants and supports: a) Zygomatic reconstruction, b) Knee prosthesis, the red squares represents the investigated areas by SEM and EDX

In concordance with other studies focussed on reducing the balling effect [51], the SLM manufacturing was done with 0.2% content of oxygen, 133W laser power and 344mm/s scanning speed for outer boundary scanning. In these SLM conditions, the granule size was reduced to 10  $\mu\text{m}$ , and the balling effect initiation was limited (Fig. 5).

According to the experimental results, when the powder is partly melted, the laser seldom scattered in the powder and the non-melted granules remain in the original (Figure 5). This observation suggests that the laser scattering is not in isotropism, but shows a strong forward tendency like in other research from the literature [45].

Figure 6 shows the SEM images with the implant surfaces after the alumina sandblasting process. There is a limitation of the striations on Ti implants and an improvement in the surface quality.

The Ti surface shows suitable multi-level structure morphology (Figure 6b). The dark areas shown in Figure 6b correspond to the particles used to sandblast these implants, especially alumina. These areas were also investigated by EDS and the chemical composition of the surface is presented in Table 1.

Following the EDS compositional analysis, multiple areas were identified, where after sandblasting, there are particles of alumina deposited on the Ti surfaces (Table 1, Spectrum 8, 9, 10, 11, 13, 14 and 15). In addition to these, other chemical elements such as Fe, Si, Cu, Cl or K have been identified on the surfaces. These chemical elements appeared forasmuch the supports were manually remove from the implant surfaces and also because it were

cleaning with a wire brush. Although the powder has been recycled many times, the Ti purity was not affected, it still remaining at 99.5% (Table 1, Spectrum 19, 20, 21).

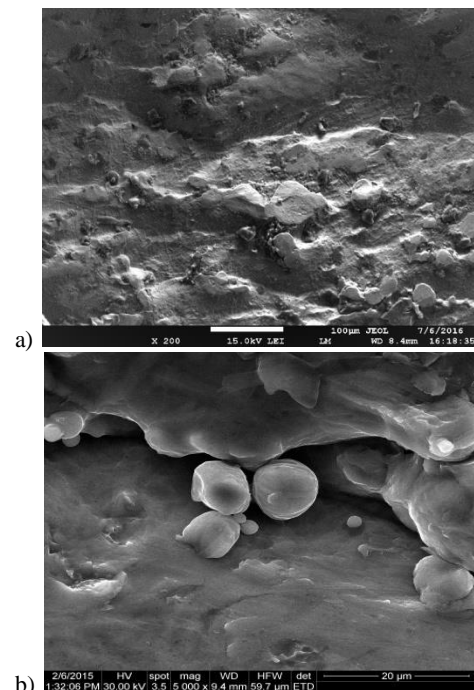


Fig. 5. a) SEM analysis of the initial surface obtained by SLM technology (500x magnification), b) Ti granules partially anchored to the surface (5000x magnification)

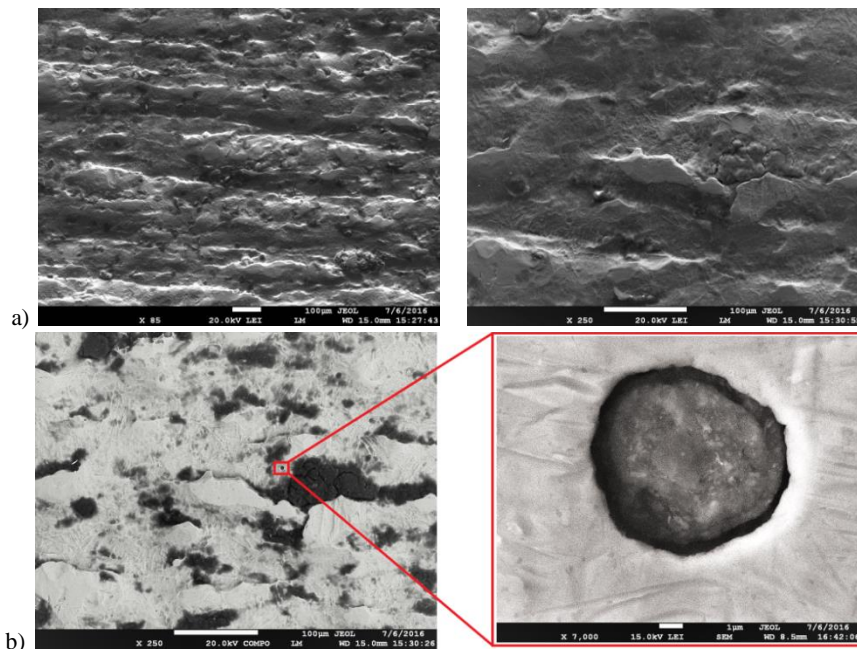


Fig. 6. a) SEM analysis after alumina sandblasting (85x and 250x magnification), b) Areas with alumina anchored onto the surface (250x and 7000x magnification)

Table 1. Chemical composition of surface after sandblasting with alumina

Spectrum label	Element weight [%]									
	Ti	Al	O	K	Cl	Si	Fe	Ni	Cu	Zn
Spectrum 8	32.7	24.1	31.6	1.5	2.3		3.7	0.5	2.1	1.4
Spectrum 9	12.0	35.7	36.0	2.0	2.8	2.1	5.1		2.3	
Spectrum 10	33.5	24.0	30.5	1.1	1.2	1.0	3.1	2.0	2	1.2
Spectrum 11	40.1	19.1	23.8	1.1	1.4	0.9	3.8	3.2	5.7	
Spectrum 12	20.0	17.6	46.5	0.5	0.6	7.3	1.9	0.2	0.9	0.6
Spectrum 13	31.4	23.0	39.2	0.5	0.9		2.6	0.3	1.2	0.8
Spectrum 14	65.6	6.9	23.3	0.2	0.5	0.4	1.6	0.2	0.9	0.4
Spectrum 15	6.1	47.5	31.3	1.1	1.5	1.0	5.5	0.7	2.4	1.6
Spectrum 16	84.5	2.2	13.3							
Spectrum 17	81.2	2.1	16.7							
Spectrum 18	99.0	0.9								
Spectrum 19	99.5	0.5								
Spectrum 20	99.5	0.4								
Spectrum 21	99.5	0.5								

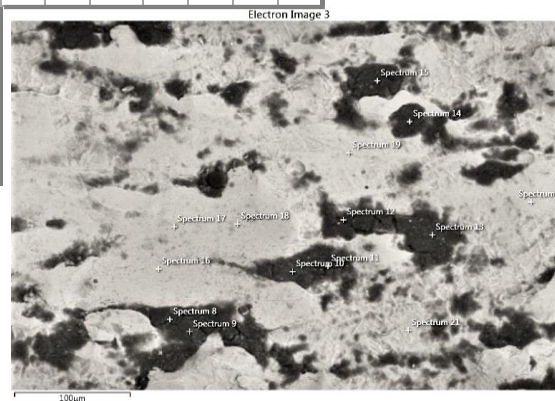


Fig. 7 investigates the surface topography after a complete post-processing of the implants (including sandblasting, polishing and ultrasonication). The surface remained homogeneous, cleaned to a large extent of partially melted particles, while improving the surface quality. In the contact areas between the part and supports that anchor it, there are micro-grooves, but their depth is limited without any accent trace (Fig. 7). The surface topography could ensure bone adhesion and good absorption of molecules from the biological fluids [52].

*In vivo* tests have demonstrated that these micro-porous

surfaces can promote a better and faster osseointegration as compared to the smooth surfaces [53], [54], [55].

In areas with lattice structures, where polishing was difficult, there are still Ti granules partially anchored on the surfaces, as it can be seen in Fig. 8. The EDX composition analysis (Spectrum 1 – Fig. 8) highlights that it is a Ti granule. After the carborundum polishing and ultrasonication, no traces of alumina on the Ti surfaces were observed, the aspects being revealed by the energy-dispersive X-ray spectroscopy analysis (Fig. 9).

### 3.3. Roughness measurements and geometrical inspection

Due to the complex forms of the implants processed by SLM, the initial  $R_a$  roughness was between 6.5-8 $\mu\text{m}$ . Following the application of the three post-processing methods detailed, the  $R_a$  was uniformed throughout the implant surface, being reduced to about 1.2  $\mu\text{m}$ . As already suggested, this micro-porous surface has a suitable relief for bone-implant interface [56]. It represents an optimal environment for coating with new bioactive materials that initiate the differentiation, proliferation and attachment of osteoblast cells [21], [57]. Even more, the obtained surfaces after post-processing could be functionalized by coatings with various bioresorbable or biodegradable materials [57], [58], [59], [60], [61]. Applying these coatings it could be enhanced the formation of new bone structures, transforming the Ti implants from bioinert into bioactive.

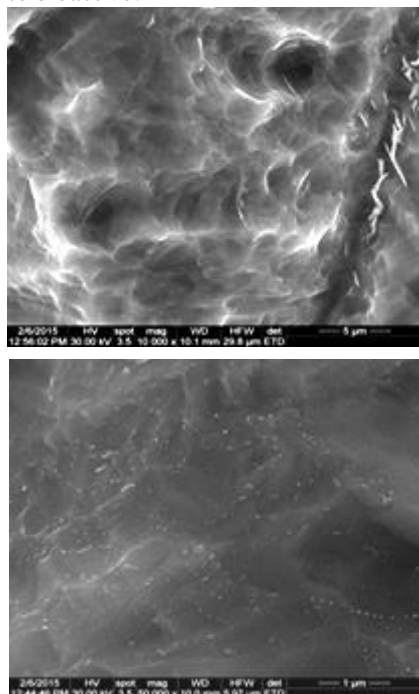


Fig. 7. SEM analysis after a complete post-processing, micro-porous areas at the contact between the implant and the supports (10,000x and 50,000 magnification)

The accuracy of the post-processed surfaces was verified by comparing the 3D scanned models with the designed implants. This procedure is part of reverse engineering and it was implemented on various medical applications because the patient needs to receive a product tailor made to their unique characteristics [62]. The results are shown in diagrams (Fig. 10) and represent a colour deviation map between the 3D CAD model (set as reference model) and the mesh captured by 3D scanning of the implants processed by solid laser.

While analyzing the accuracy of the surfaces which were anchored with supports, the maximum positive deviation is +0.29 mm for zygomatic implant and +0.48mm on knee prostheses.

The maximum negative deviation is -0.35 mm for zygomatic implant and -0.46 mm on knee prostheses. In order to highlight the existing geometrical average deviations, the histogram is displayed in addition to the colour scale shown in Figure 10. This histogram is a graphical representation of the frequency distribution of scaled characteristics. The average deviation is +0.03 mm for zygomatic implant, respectively +0.07 mm on knee prostheses.

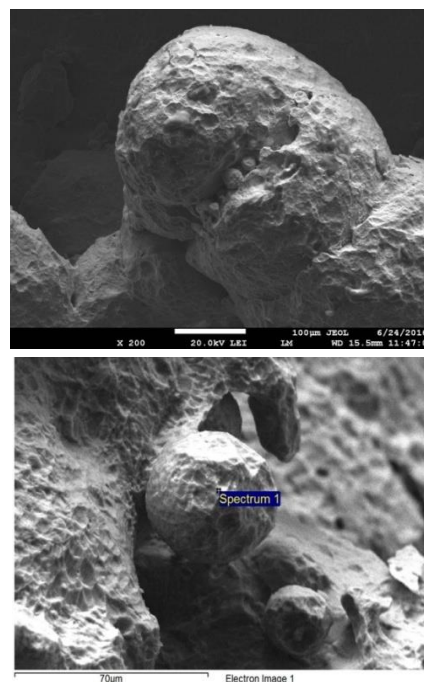


Fig. 8. SEM analysis of the lattice structure after a complete post-processing (200x and 500x magnification)

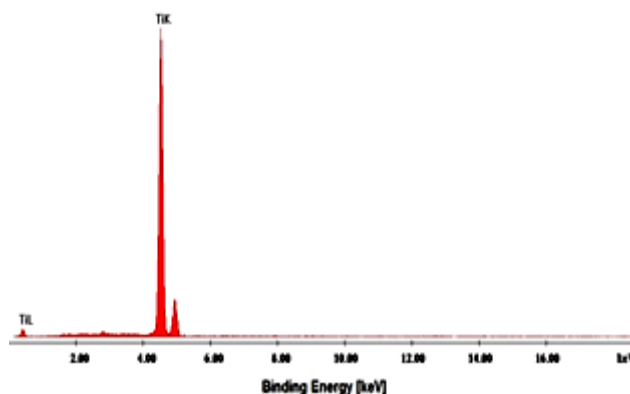


Fig. 9. Energy-dispersive x-ray spectroscopy of implants after the post-processing was completed

According to this study and other research [15], [49], the outer boundary has indicated a higher deviation since it was warped due to thermal stress. In general, proper supports effectively prevent the warpage effect, and deviations between  $\pm 0.12$  mm could be expected (see Fig. 10). On a thorough inspection of the post-processed implants, minor imperfections were observed on the surfaces where there was a direct contact with the supports.

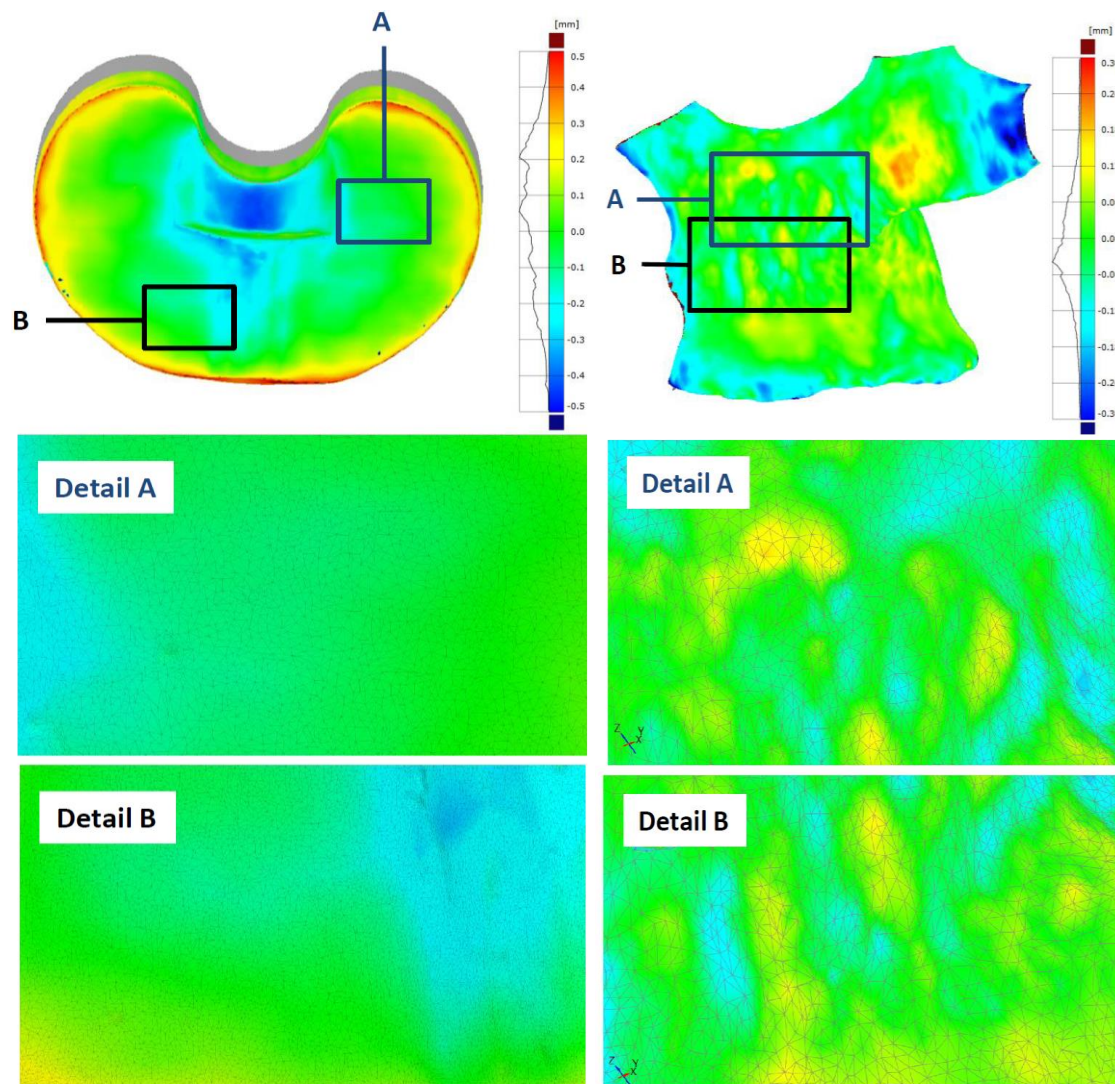


Fig. 10. Comparison diagrams between 3D model and SLM-manufactured implant, zygomatic implant (left side) and tibial component (right side)

The post-processing of the contact surface between the implant and the support structures is essential, and special care must be taken to have acceptable accuracy limits especially when the implants SLM-manufactured were not exposed to a stress relieved treatment. This research demonstrates that the optimal SLM process parameters for pure Ti can limit the level of residual stress, avoiding the deformation defects of complex shapes without any thermal treatment after manufacturing.

Combining these three post-processing methods, the quality of complex surfaces which had supports attached is significantly improved, and it can be considered as a low cost post-processing because it does not add significant fee to SLM processed implants. At the same time they are efficient if their order is respected.

#### 4. Conclusions

The SLM technology is capable to produce directly medical implants with anatomical forms, including those

with lattice-controlled structures that can support long-term bone ingrowth (osseointegration). With detailed process parameters, the Nd:YAG laser scanning at 1064nm was efficient and the beam quality was also improved. The SLM process was stable and no defects occurred in the Ti implants. By reducing the oxygen level during the laser scanning and proper configuring of process parameters, the balling effect was limited on outer contour of the parts. The SEM analyses have revealed that on the initial surfaces of the implants, granules with small diameter were sometimes partially-anchored.

The study presented a new approach focused on post-processing of the implants made by laser beam melting. The post-processing was done with alumina sandblasting, carborundum discs polishing and ultrasonication in isopropyl alcohol. The proposed post-processing technologies are not expensive, they can become efficient when are combined and significantly improve the quality of the anatomical surface which has supports attached. Following the alumina sandblasting, on the Ti surfaces granules from the abrasive material are found on it. After

carborundum polishing and ultrasonification, the SEM investigations have shown that the implant surfaces are homogenous and they are mainly cleaned of partially anchored Ti or alumina granules. Using these three post-processing methods, the EDX spectrums revealed that the Ti surfaces are not contaminated with other materials.

The post-processing technologies have contributed to the uniformization and reducing of the  $R_a$  roughness on all the implant surfaces. Furthermore, the surfaces anchored with supports had limited deviation accuracy. Setting up the optimal process parameters of Nd:YAG solid laser, the residual stress effect on the precision has been also limited, even if the implants were not subjected to a thermal stress relieved treatment. The obtained results provide two case references for directly manufacturing and post-processing of complex customized implants, which could be applied in maxillofacial surgery and total knee arthroplasty.

### Acknowledgments

This paper was supported by the OpTi-DeP Project (no. BG101/2016) financed from the UEFISCDI by the Romanian Government, and within the H2020 AMaTUC project (GA 691787). Also this publication is the result of the project implementation: CE for development and application of advanced diagnostic methods in processing of metallic and non-metallic materials - APRODIMET, ITMS: 26220120048, supported by the Research & Development Operational Programme funded by the ERDF Slovakia.

### References

- [1] J. Imanishi, P. F. Choong, T. Int. J. Surg. Case. Rep. **10**, 83 (2015).
- [2] J. Parthasarathy, Ann Maxillofac. Surg. **4**, 9 (2014).
- [3] D. V. Leordean, C. Dudescu, T. Marcu, P. Berce, N. Balc, Rapid Prototyping J. **21**, 1 (2015).
- [4] D. Leordean, S.A. Radu, D. Frătilă, P. Berce, Int J. Adv. Manuf. Tech. **79**, 5 (2015).
- [5] T. Marcu, M. Todea, L. Maines, D. Leordean, P. Berce, C. Popa, Powder Metall. **55**, 4 (2013).
- [6] T. Marcu, C. Menapace, L. Girardini, D. Leordean, C. Popa, Rapid Prototyping J. **20**, 4 (2014).
- [7] Y. Zhang, F. Liu, J. Chen, Y. Yuan, Journal of Laser Applications **29**, 022306 (2017).
- [8] V. Seyda, D. Herzog, Journal of Laser Applications **29**, 022311 (2017).
- [9] L.E. Murr, S.M. Gaytan, E. Martinez, F. Medina, R. B. Wicker, International Journal of Biomaterials **2012**, DOI:10.1155/2012/245727 (2012).
- [10] I. Kroonenburgh, I. Lambrechts, J. Poukens, Digital Dental News **04**, 60 (2012).
- [11] H. Rotaru, R. Schumacher, S. Kim, C. Dinu, Maxillofacial Plastic and Reconstructive Surgery **37**(1), 1 (2015).
- [12] T. Nakano, T. Ishimoto, KONA Powder and Particle Journal **32**, 75 (2015).
- [13] M. Kaya, A. Buğutekin, N. Orhan, Optoelectron. Adv. Mat. **4**(8), 1250 (2010).
- [14] Y. Liu, Y. Yang, D. Wang, Int. J. Adv. Manuf. Technol. **87**, 647 (2016).
- [15] C. Song, Y. Yang, Y. Wang, et al., Int J. Adv. Manuf. Technol, **75**, 445 (2014).
- [16] R. Pacurar, N. Balc, F. Prem, Proceedings of 14<sup>th</sup> International ESAFORM Conference on Material Forming. AIP Publishing, **1353**(1), 1385 (2011).
- [17] J. P. Kruth, E. Yasa, J. Deckers, Proceedings of the 3rd International Conference on Polymers and Moulds Innovations (2008).
- [18] A. Gebhardt, J. Hötter, D. Ziebura, R. Tejournal Forum für Rapid Technologie (2014).
- [19] I. Vijay-Arasu, K. Chockalingam, C. Kailasanathan, M. Sivabharathy, International Journal of Chem. Tech. Research **6**(5), 2993 (2014).
- [20] M. M. Wood, E. M. Warshaw, Dermatitis **26**(1), 7 (2015).
- [21] S. V. Savu, I. D. Savu, G. C. Benga, I. Ciupitu, Optoelectron. Adv. Mat. **10**(9-10), 752 (2016).
- [22] T. Laoui, E. Santos, K. Osakada, M. Shiomi, M. Morita, S.K. Shaik, N.K. Tolochko, F. Abe, M. Takahashi, J. Mechanical Engineering Science, Proc. IMechE 220, Part C: 857 (2006).
- [23] G. Li, L. Wang, W. Pan, et al., Scientific Reports **6**, 34072 (2016).
- [24] M. Toth-Tascau, D. I. Stoia, Optoelectron. Adv. Mat. **5**(12), 1356 (2011).
- [25] J. Banhart, Functional applications, Handbook of cellular metals: Production, Processing, Applications, Ed. Wiley-VCH Verlag, Weinheim, 2002.
- [26] A. Shehata, W. Bleck, P. Scholz, Metal Powder Report **60**, 38 (2005).
- [27] I. Gligor, T. Marcu, M. Todea, L. Conț, V. Căndea, C. Popa, J. Optoelectron. Adv. M. **13**(7), 879 (2011).
- [28] J. P. Li, S. H. Li, C. A. Blitterswijk, K. Groot, Journal of Biomedical Materials Research **73**(A), 223 (2005).
- [29] A. Nouri, P. D. Hodgson, C. Wen, "Biomimetic Porous Titanium Scaffolds for Orthopedic and Dental Applications, Biomimetics Learning from Nature", Ed. Amitava Mukherjee - InTech, 2010.
- [30] M. Bram, H. Schiefer, D. Bogdanski, M. Köller, H. P. Buchkremer, D. Stöver, Metal Powder Report, **61**, 26 (2006).
- [31] Z. Esen, S. Bor, Scripta Materialia **56**, 341 (2007).
- [32] D. Xin, C. Na, et al., Chinese Physics Letters **26**, 9 (2009).
- [33] X. Wang, T. Zuo, Front. Optoelectron. China **3**(2), 190 (2010).
- [34] A. Ispas, C. Cosma, A. Craciun, M. Constantiniuc, L. Lascu, D. Leordean, C. Vilau, J. Optoelectron. Adv. M. **18**(9-10), 904 (2016).
- [35] P. Magne, U. C. Belser, Int J Periodontics Restorative Dent **22**(5), 425 (2002).
- [36] N. Balc, S.C. Cosma, J. Kessler, V. Mager, Applied Mechanics and Materials **808**, 199 (2015).

- [37] K. Zeng, Optimization of support structures for selective laser melting, *Electronic Theses and Dissertations.*, Paper 2221, 2015.
- [38] S. Cavalu, C. Ratiu, O. Ponta, V. Simon, D. Rugina, V. Miclaus, I. Akin, G. Goller, *Dig. J. Nanomater. Bios.* **9**(2), 797 (2014).
- [39] G. D. Byrne, L. O'Neill, B. Twomey, D. P. Dowling, *Surface & Coat Technology* **216**, 224 (2013).
- [40] S. Li, J. Ni, X. Liu, H. Lu, S. Yin, M. Rong, Z. Guo, *Materials Transactions* **53**(5), 913 (2012).
- [41] M. D. Pereda, K. W. Kang, R. Bonetto, C. Llorente, P. Bilmes, C. Gervasi, *Procedia Materials Science* **1**, 446 (2012).
- [42] L. Morovič, "Non-Contact Measurement of Free-Form Surfaces", Aleš Čeněk, Plzeň, p. 89, 2016.
- [43] T. Brajlili, T. Tasic, et al., *Journal of Mechanical Engineering* **57**(11), 826, (2011).
- [44] Y. B. Band, "Light and Matter: Electromagnetism, Optics, Spectroscopy and Lasers", Ed. Wiley, 2006, ISBN: 978-0-471-89931-0.
- [45] X. Wang, H. Yuan, M. Wang, W. Huang, *Optics Communications*, **376**, 67 (2016).
- [46] C. Cosma, „Research on Improving the Manufacturing of Titanium Medical Implants, by Selective Laser Melting - PhD thesis”, Technical University of Cluj-Napoca, 2015.
- [47] J. B. Berger, H. N. G. Wadley, R. M. McMeeking, *Nature* **543**, 533 (2017).
- [48] V. A. Ceclan, I. A. Popan, S. D. Grozav, C. Miron-Borzan, I. Kuric, *Applied Mechanics and Materials* **808**, 286 (2015).
- [49] L. C. Zhang, H. Attar, *Advanced Engineering Materials* **18**(4), 463 (2016).
- [50] R. Li, J. Liu, Y. Shi, L. Wang, Wei Jiang, *Int. J. Adv. Manuf. Technol.* **59**, 1025 (2012).
- [51] B. Song, S. Dong, B. Zhang, H. Liao, C. Coddet, *Materials and Design* **35**, 120 (2012).
- [52] Q. Liu, H. Wang, *Tissue Regeneration: Where Nano-structure Meets Biology*, Ed. World Scientific Publishing, 2014, ISSN 2251-3965.
- [53] C. Larsson Wexell, P. Thomsen, B.O. Aronsson et al., *International Journal of Biomaterials* **2013**, 10 (2013).
- [54] C. Mangano, V. Perrotti, M. Raspanti et al., *International Journal of Oral & Maxillofacial Implants* **28**(3), 917 (2013).
- [55] F. Rupp, R. A. Gittens, L. Scheideler et al., *Acta Biomaterialia* **10**(7), 2894 (2014).
- [56] M. Herrero-Climent, P. Lázaro, J. Vicente Rios, S. Lluch, M. Marqués, J. Guillem-Martí, F. Gil, *J. Mater Sci Mater Med.* **24**(8), 2047 (2013).
- [57] E. Andronescu, F. M. Iordache, C. S. Ciobanu, M. L. Badea, A. Costescu, A. M. Prodan, *Optoelectron. Adv. Mat.* **9**(9-10), 1155 (2015).
- [58] G. Zegan, R. Cimpoesu, M. Agop, I. Știrbu, D. L. Chicet, B. Istrate, A. Alexandru, B. Anton Prisacariu, *Optoelectron. Adv. Mat.* **10**(3-4), 279 (2016).
- [59] G. Armencea, C. Berce, H. Rotaru, et al., *Optoelectron. Adv. Mat.* **9**(5-6), 865 (2015).
- [60] M. Moldovan, C. Prejmerean, D. Prodan, L. Slilaghi Dumitrescu, R. Carpa, S. Pruneanu, C. Sarosi, *Dental Materials*, **33**(1), e54 (2017).
- [61] A. Burde, S. Cuc, A. Radu, M. Rusu, C. Cosma, D. Leordean, *Studia UBB Chemia* **LXI**, 2 (2016).
- [62] R. Racasan, D. Popescu, C. Neamtu, M. Dragomir, *Automation Quality and Testing Robotics (AQTR), IEEE International Conference*, p. 461 (2010).

---

\*Corresponding author: cosmin.cosma@tcm.utcluj.ro